Highlights of OH, H_2SO_4, and methane sulfonic acid measurements made aboard the NASA P-3B during Transport and Chemical Evolution over the Pacific

R. L. Mauldin III,[1] C. A. Cantrell,[1] M. Zondlo,[1,2] E. Kosciuch,[1] F. L. Eisele,[1,3] G. Chen,[3,4] D. Davis,[3] R. Weber,[3] J. Crawford,[4] D. Blake,[5] A. Bandy,[6] and D. Thornton[6]

Received 14 January 2003; revised 29 April 2003; accepted 19 May 2003; published 29 October 2003.

[1] Measurements of hydroxyl radical (OH), sulfuric acid (H_2SO_4), and methane sulfonic acid (MSA) were performed aboard the NASA P-3B using the selected ion chemical ionization mass spectrometry technique during the Transport and Chemical Evolution over the Pacific (TRACE-P) study. Photochemical box model calculations of OH concentrations yielded generally good agreement with an overall tendency to overestimate the measured OH by ~20%. Further analysis reveals that this overestimation is present only at altitudes greater than ~1.5 km, with the model underestimating OH measurements at lower altitudes. Boundary layer H_2SO_4 measurements, performed in a volcanic plume off the southern coast of Japan, revealed some of the largest marine boundary layer H_2SO_4 concentrations ever observed and were accompanied by new particle formation. Nighttime measurements of OH, H_2SO_4, and MSA in the remote pacific off Midway Island revealed significant boundary layer concentrations of H_2SO_4 and MSA, indicating evidence of nighttime boundary layer oxidation processes but in the absence of OH. A cursory exploration of the sources of production of the H_2SO_4 and MSA observed at night is presented. *INDEX TERMS:* 0317 Atmospheric Composition and Structure: Chemical kinetic and photochemical properties; 0365 Atmospheric Composition and Structure: Troposphere—composition and chemistry; 0370 Atmospheric Composition and Structure: Volcanic effects (8409); *KEYWORDS:* TRACE-P, hydroxyl, oxidation

Citation: Mauldin, R. L., III, et al., Highlights of OH, H_2SO_4, and methane sulfonic acid measurements made aboard the NASA P-3B during Transport and Chemical Evolution over the Pacific, *J. Geophys. Res.*, *108*(D20), 8796, doi:10.1029/2003JD003410, 2003.

1. Introduction

[2] The NASA Global Tropospheric Experiment (GTE) Transport and Chemical Evolution over the Pacific (TRACE-P) study offered a unique opportunity to perform OH, H_2SO_4, and methane sulfonic acid (MSA) measurements over a wide variety of environments and conditions. The study was conducted February–April 2001, with five flights out of Hong Kong, China, and six flights out of Yakota, Japan [*Jacob et al.*, 2003]. Transit flights to and from Asia allowed measurements to be performed in remote marine environments across the Pacific, while flights off the eastern coast of Asia allowed air masses with continental origins to be sampled. This Asian outflow could produce air masses perturbed with high levels of NO_x, SO_2, CO, CH_4, and numerous other hydrocarbons.

[3] In these regions the hydroxyl radical (OH) will be one of the primary cleansing or oxidizing agents, significantly controlling the chemical evolution of air masses during transport. Through multistep reactions, OH is responsible for the removal of most atmospheric carbon containing compounds (CO, CH_4, nonmethane hydrocarbons), either anthropogenic or biogenic in origin, and their subsequent oxidation products. These reactions ultimately lead to the formation of H_2O and CO_2. The lifetime of these organic species is determined in large part by the concentration of OH. Thus, in part, OH controls how carbon is partitioned between the product CO_2 and organic emissions like CH_4 and intermediates such as CO (also a direct emission) at any given time after reactive carbon enters the atmosphere.

[4] H_2SO_4 is produced by the OH-initiated oxidation of SO_2. Natural sources of SO_2 include oxidation of reduced sulfur (DMS) emitted by the ocean and direct volcanic emission. Large quantities of SO_2 are also produced on the Asian continent from the use of high sulfur coal as a fuel source. Once in the atmosphere, much of this SO_2 is oxidized by OH to ultimately form H_2SO_4. Once formed, gas phase H_2SO_4 plays an important role in governing the rate of new particle formation and particle growth rates and ultimately cloud condensation nucleus (CCN) production

[1]Atmospheric Chemistry Division, National Center for Atmospheric Research, Boulder, Colorado, USA.
[2]Now at Southwest Sciences, Inc., Santa Fe, New Mexico, USA.
[3]School of Earth and Atmospheric Sciences, Georgia Institute of Technology, Atlanta, Georgia, USA.
[4]Now at NASA Langley Research Center, Hampton, Virginia, USA.
[5]Department of Chemistry, University of California, Irvine, Irvine, California, USA.
[6]Department of Chemistry, Drexel University, Philadelphia, Pennsylvania, USA.

0148-0227/03/2003JD003410$09.00

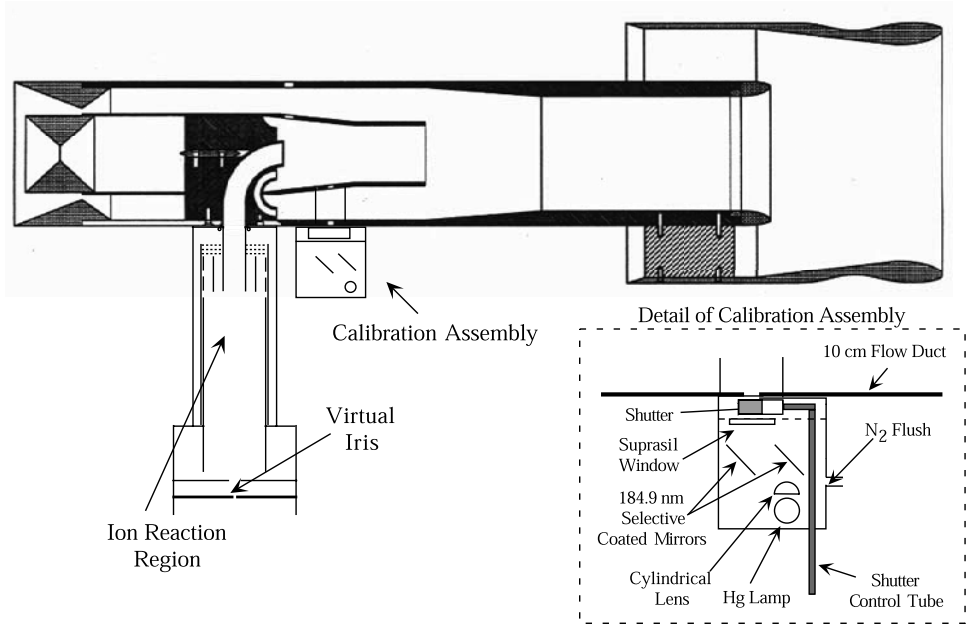

Figure 1. Schematic diagram of the Selected Ion Chemical Ionization Mass Spectroscopy (SICIMS) instrument used for the measurement of OH, H_2SO_4, and methane sulfonic acid (MSA) during Tropospheric Experiment Transport and Chemical Evolution over the Pacific (TRACE-P). The inset shows the calibration source used for the in situ generation of OH.

and cloud properties. In remote regions the aerosols and CCN produced by these nucleation and growth processes can reduce visibility and affect climate [*Charlson et al.*, 1987; *Twomey et al.*, 1984].

[5] In the remote marine environment, MSA is produced via the oxidation of DMS [*Davis et al.*, 1998]. Once in the atmosphere, DMS is oxidized by OH via a branched mechanism to produce either SO_2, much of which eventually forms H_2SO_4, or products which can lead to the formation of MSA [*Ayers et al.*, 1991; *Yin et al.*, 1990; *Toon et al.*, 1987; *Hatakeyama et al.*, 1982]. Once formed, gas phase MSA has a lifetime similar to that of H_2SO_4, being lost to surfaces or rainout [*Ayers et al.*, 1991; *Yin et al.*, 1990]. Recent results from the Tropospheric Ozone Production about the Spring Equinox (TOPSE) study have shown MSA to be present in air masses with anthropogenic influences [*Mauldin et al.*, 2003].

[6] Here we present highlights of OH, H_2SO_4, and MSA measurements made aboard the NASA P-3B during the TRACE-P study. Overall model comparisons of OH will be discussed. H_2SO_4 data from a flight through a volcanic plume off the southern coast of Japan will be presented. Additionally, some very interesting results from a nighttime flight in the remote marine environment out of Midway Island will be presented.

2. Data Acquisition and Analysis

[7] Measurements of OH, H_2SO_4, and MSA were performed aboard the NASA P-3B using the selected ion chemical ionization mass spectroscopy (SICIMS) technique. A schematic diagram of the instrument used in this study can be found in Figure 1. The system consists of three major sections: a shrouded inlet which straightens and slows the air flow, an ion reaction region in which the chemical ionization reactions occur, and a turbo molecular pumped vacuum chamber which houses a quadrupole mass spectrometer and an electron multiplier detector. The measurement technique and system used in this study have been described in detail elsewhere [*Eisele and Tanner*, 1991, 1993; *Tanner et al.*, 1997; *Mauldin et al.*, 1998, 1999]; therefore the reader is directed to those works for experimental details.

[8] The same calibration assembly and technique as described by *Mauldin et al.* [2001] were employed in the measurements presented here. Briefly, the technique involves the photolysis of H_2O at 184.9 nm to produce a known amount of OH in front of the 1.9 cm curved sampling inlet. As shown in Figure 1, light from a Pen Ray Hg lamp passes through a cylindrical lens (Suprasil), reflects off of two mirrors coated to selectively reflect 184.9 nm, and then exits the calibration assembly via a Suprasil window and shutter/slit mechanism. The light then passes through an enclosed 2.5 cm path before illuminating the sample flow. To prevent light absorption and the buildup of O_3 within the calibration assembly, the calibration housing was purged with N_2. As OH is converted to, and measured as, $H_2{}^{34}SO_4$, this calibration also serves as a calibration for ambient H_2SO_4 and MSA [*Eisele and Tanner*, 1991].

[9] The OH concentration produced by the calibration source is a function of the intensity of the photon flux at 184.9 nm, the $[H_2O]$, the absorption cross section at 184.9 nm, the yield of OH from H_2O photolysis, and the sample flow velocity. The flow velocity was measured using a Pitot tube mounted just forward of the 1.9 cm curved inlet, and the $[H_2O]$ was measured using a dew point hygrometer aboard the aircraft. To determine the photon flux from the lamp at 184.9 nm, vacuum UV photo diodes mounted on an

x/*y* traverse were used to periodically map out the light field on the ground. The quantum efficiency of these diodes was compared to a National Institute of Standards and Technologies (NIST) standard diode both prior to and after the mission and were found to vary at the ±12% level. A value of 7.14×10^{-20} cm^2 molecule was used for the H_2O absorption cross section at 184.9 nm [*Cantrell et al.*, 1997].

[10] Problems arose with the implementation of this technique. Upon installation, the assembly was checked and appeared to be working correctly. However, prior to deployment a leak developed between the Suprasil window and the calibration housing, allowing ambient air to enter the housing. The leak was identified by viewing the time history of the measured calibration values. Unfortunately, this leak was not detected until after the study. Briefly stated, this leak caused the following problem. Normally the photon fluence at 184.9 nm is determined from diode mappings performed in front of the 1.9 cm curved inlet while the plane is on the ground. The light exiting the lamp assembly is then calculated by increasing the mapping values to account for absorption due to ambient O_2 and H_2O over the 7.26 cm path to the curved inlet. It should be pointed out that the combined photon fluence measurements from all diodes varied by ±15% (2 sigma) throughout the entire study, indicating that the lamp output was stable and the quality of the optics did not degrade significantly. For in situ calibrations the photon fluence at the 1.9 cm curved inlet is calculated by decreasing the flux value at the lamp exit to account for absorption due to ambient O_2 and H_2O over the 7.26 cm path to the curved inlet for the conditions under which the calibrations were performed. The leak in the calibration assembly produced a problem in this calculation. While on the ground, the leak in the calibration assembly had little effect. Typically, winds were light and the assembly had been left purging with N_2 for several hours before diode mappings were performed. Under these conditions the housing appeared to be fully flushed with N_2. However, once airborne, exposure to winds of >100 m s^{-1}, and pressure changes associated with changing altitude, allowed the interior to fill with ambient air, resulting in additional attenuation of 184.9 nm light exiting the assembly due to absorption from O_2 and H_2O within the lamp assembly itself. The leak appears to be so large as to make the purge N_2 added negligible. If not accounted for, this attenuation causes an overestimate of the calculated amount of OH produced by the calibration assembly, which results in a calibration coefficient which overestimates ambient OH.

[11] It should be possible to correct for the effects of this leak using the same approach as used in calculating the photon flux from the lamp. If the flux exiting the lamp assembly, calculated from the ground-based diode mappings with the assembly fully purged with N_2, is assumed to be the flux produced by the lamp, this value can then be corrected to account for the additional absorption, caused by the leak, occurring over the path length within the lamp assembly. One drawback to this approach is that the absorption cross section for O_2 is dependent upon both the lamp characteristics and O_2 column concentration [*Creasey et al.*, 2000]. As pointed out by these authors, to accurately use this technique, it is necessary to measure the O_2 absorption cross section at the various O_2 column concentrations under which the calibrations were performed. Thus laboratory tests were performed where the O_2 absorption cross section was measured. A mechanical determination of the path length within the lamp assembly yielded a value of 7.31 cm. An apparatus was constructed such that the O_2 absorption cross section could be determined over a 7.26 or 14.57 (7.26 + 7.31) cm path length. Three identical Hg Pen Ray lamps and power supplies to that used in the calibration assembly were employed. (Mounting considerations prevented the use of the actual lamp and power supply.) Light intensity at 184.9 nm was measured using a solar blind photo diode. The entire lamp/absorption cell/detector assembly was placed in an N_2-flushed housing. O_2 column concentrations were varied in the $2 - 85 \times 10^{18}$ molecule cm^2 range. Tests performed either with or without a 184.9 band-pass filter yielded identical results. The use of different lamp/power supply combinations yielded a 2 sigma standard deviation of ±16%. O_2 column concentrations of 20 and 75×10^{18} molecule cm^2 (the same column concentration range as field determinations, either in situ calibrations or diode mappings, were performed under) yielded cross sections of 12.3 and 8.6×10^{-21} cm^2 molecule respectively. The measured cross section for an O_2 column of 5.5×10^{18} molecule cm^2 is $1.48 \pm 0.23 \times 10^{-20}$ cm^2 molecule, a value in reasonable agreement with the results of *Creasey et al.* [2000], *Hofzumahaus et al.* [1997], and *Lanzendorf et al.* [1997], who obtained values between 1.1 and 1.4×10^{-20} cm^2 molecule.

[12] With the O_2 column measurements in hand, the correct calibration coefficients could be calculated. Figure 2 is a plot of the calibration coefficients determined from this study versus ambient pressure. The points shown in Figure 2 are the average values for each calibration performed, with error bars showing the calculated standard deviation (2 sigma). There are two fits shown on the plot (Figure 2). The solid line in Figure 2 is the fit to the calibration values obtained in this study. This fit yielded values ~25–30% larger than those obtained in previous studies. The calibration factor is not a highly variable quantity, depending upon the ion source geometry, ion reaction time, and detection sensitivity. This same OH, H_2SO_4, and MSA instrument configuration was also flown aboard the P3-B during the GTE Pacific Exploratory Mission-Tropics B (PEM-Tropics B) study. Operationally, differences in lens voltages (which affect ion reaction times) as a function of altitude prevent comparison at all altitudes; however, at sea level, identical lens voltages (ion reaction times) were used. At this altitude, calibration values of 12.46 and 10.19 molecule cm^{-3} are obtained from the fits used for TRACE-P and PEM-Tropics B, respectively. A sea level value of ~10 molecule cm^{-3} was also obtained from similar but not identical instrument configurations during the National Science Foundation First Aerosol Characterization Experiment (ACE-1) and GTE Pacific Exploratory Mission-Tropics A (PEM-Tropics A) studies. As this value is not expected to change, the ~22% difference from historical values observed here is probably attributable to the correction for the leak in the calibration calculation. One possible cause is the assumption that the assembly was filled with air at ambient conditions. The composition of the air within the assembly, particularly H_2O, is probably different than ambient due to changes in ambient pressure

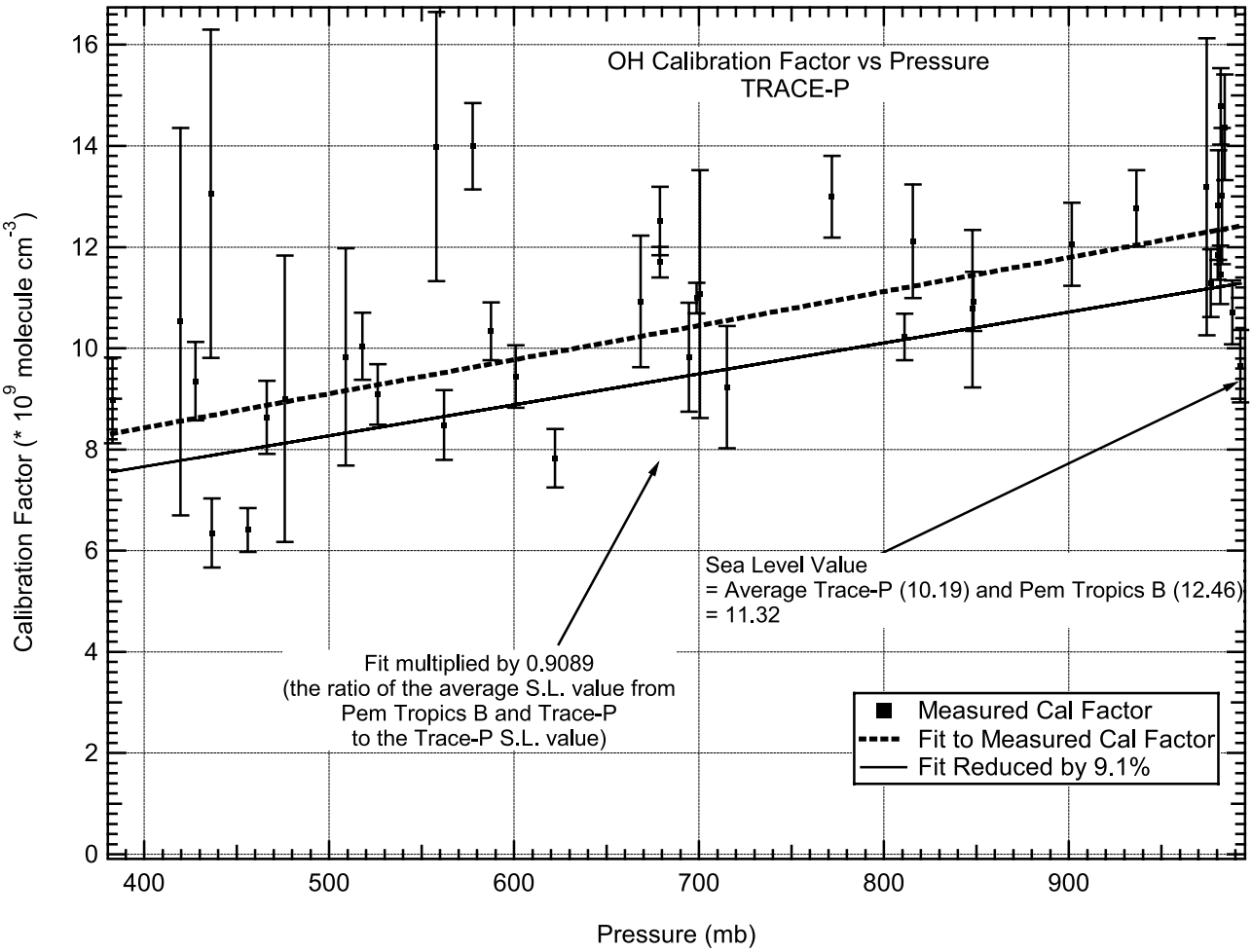

Figure 2. Plot of the calibration coefficient versus altitude for calibrations obtained during the TRACE-P study. These values have been corrected for the calibration assembly leak (see text). Also shown is the fit to these values together with a fit which has been reduced by ~9%, to obtain a sea level value which is the average of the sea level values obtained in this study and the Pacific Exploratory Mission-Tropics B (see text).

(altitude). Additionally, there was also probably a buildup of ozone within the assembly. If the ozone concentrations reached sufficient levels, it could cause additional attenuation of the lamp output.

[13] With the knowledge that the calibrations in the present study had additional corrections made to them, combined with the historical consistency of the calibration coefficient, the decision was made to reduce the fit for the present calibration values by 11%, such that the new sea level value is the average of the values from the present study and PEM-Tropics B. This corrected fit is shown as the dashed line in Figure 2. OH, H_2SO_4, and MSA values reported for this study were calculated using this lowered "average" fit.

[14] It should also be pointed out that there was a larger than normal spread in the comparisons of the measurement diodes with the NIST standard diode. This spread of approximately ±12% is about a factor of 3 larger than previously observed and is thought to be attributed to changes in the operation of the measurement apparatus. The total reported error limits are typically ±60% (2 sigma), with exceptions due to instrumental problems. The error value includes the ±40% calculated from a propagation of errors calculation which includes both the total systematic and random errors for a given measurement and an additional ±20% to reflect the spread of the NIST comparisons and the use of the corrected fit. Further, the 11% change to the fit falls well within the original ±40% error limits.

3. Results and Discussion

3.1. OH Measurements and Model Comparison

[15] The results of OH, H_2SO_4, and MSA measurements performed aboard the P-3B during TRACE-P can be found in the GTE data archive at http://www-gte.larc.nasa.gov/trace/TP_dat.htm. Data are presented as 30 s measurements using the same data acquisition technique as described by *Mauldin et al.* [2001]. As in previous airborne studies, most of the large scale variability in the data is due to changes in altitude. Smaller scale features which are observed during constant altitude legs are due to changes in $[H_2O]$, $j(O_3 \rightarrow O(^1D))$, and/or changes in [NO].

[16] Photochemical box model simulations of OH data were performed using a model developed at the Georgia

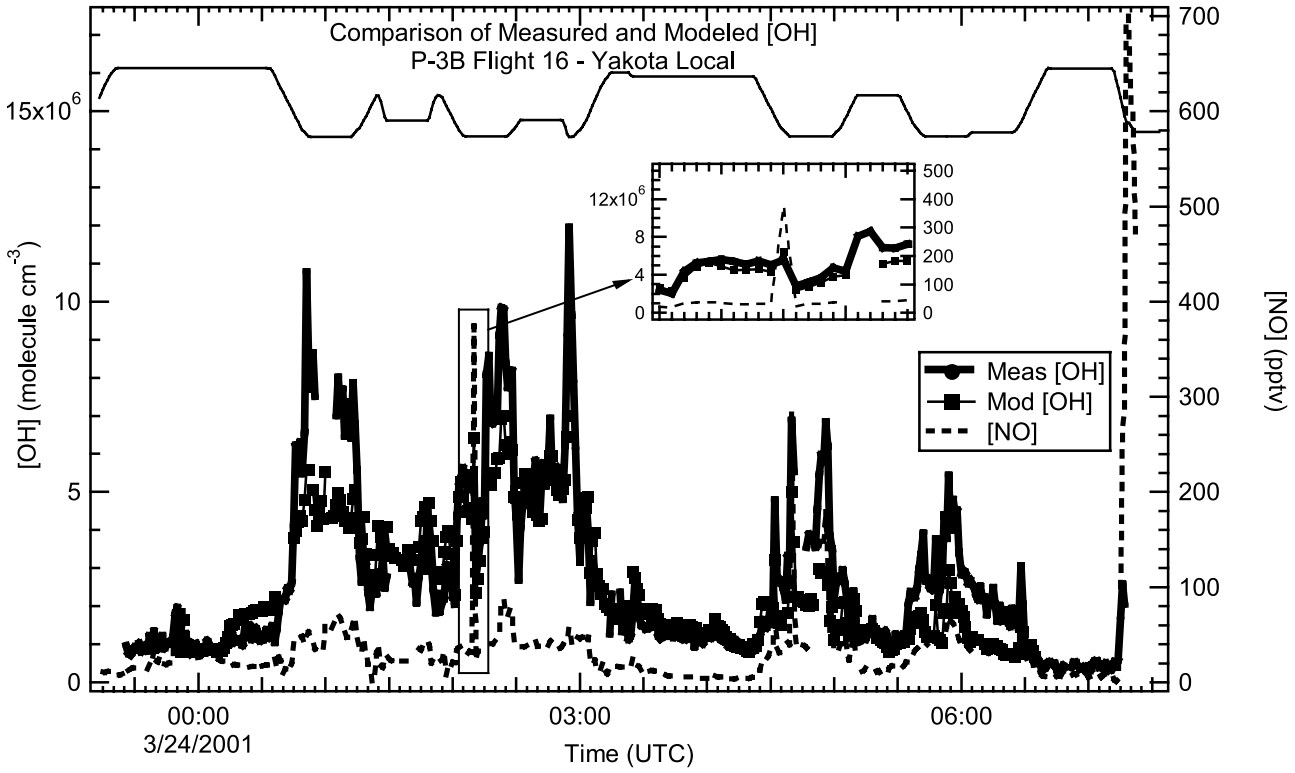

Figure 3. Plot of measured and modeled OH concentrations for a typical flight together with observed [NO], a key specie in controlling OH. A relative altitude profile (0.2–5.3 km) is provided for reference. As can be seen much of the high-frequency changes are due to changes in [NO]. The large spikes in NO (due to a ship plume) are large enough to suppress OH by acting as a sink to HO_x (see text).

Institute of Technology and enhanced at NASA Langley. A full discussion of the model used for these OH simulations and its use for the effects of clouds upon other radical species can be found in the work of [*Crawford et al.*, 2003]. The reader is directed there for model details. A typical comparison of measured and modeled [OH] for a single flight can be found in Figure 3. Also shown is a plot of [NO], a key species in controlling the cycling of HO_2/RO_2 into OH. A relative altitude profile has been added for reference. As can be seen, there are regions where the model agrees well with measurements and others where it does not. Most of the overall fine structure observed in the measurements is also seen in the modeled values. An interesting feature on this plot is the large spike of NO, from a ship plume encounter, which occurs at ~0210 UTC. When NO concentrations increase to levels up to ~150 parts per trillion by volume (pptv), OH concentrations are enhanced due to increased cycling of HO_2 back into OH. However, at NO concentrations above ~150 pptv, the accompanying NO_2 begins to act as a sink for OH via pathways that lead to the formation of HNO_3 (and HO_2NO_2). From the inset in Figure 3 it can be seen that during the NO spike the measured OH increases by ~50%, going from $\sim 4 \times 10^6$ to $\sim 6 \times 10^6$ molecule cm^{-3}. This modest increase is a combination of the enhanced cycling of HO_2 into OH and a larger sink for OH via reactions with NO_2 (and additional hydrocarbons). The flight path of the aircraft tried to follow the plume, encountering it from the up wind direction. It can be seen that following the initial encounter OH drops $\sim 6 \times 10^6$ to $\sim 2 \times 10^6$ molecule cm^{-3} and then begins a slow rise back to the value of $\sim 4 \times 10^6$ molecule cm^{-3} observed before the plume encounter. This drop is due to increased losses of OH via reactions with hydrocarbons and NO_2, which then begin to dilute, allowing OH to climb back to its preplume value. While not agreeing exactly with the measurements, the model also predicts a similar increases and decrease in OH in this highly chemically perturbed environment. A plot of measured versus modeled [OH] for flights 4–24 (all flights during the TRACE-P campaign) is shown in Figure 4. As can be seen with the exception of a few outlying points, the agreement is generally good. A linear regression with a zero intercept of this data yields a slope of 0.89. A standard regression yields a slope of 0.85 and an intercept of 5.22×10^5 molecule cm^{-3}. The slope of either regression indicates that the model has a slight tendency to overpredict OH concentrations when compared to the present measurements. This type of figure is good at revealing average overall trends; however, it is not good at elucidating specific types of dependencies. A cursory look at the agreement between measured and modeled values in Figure 3 reveals that the modeled values are lower than measurements at low altitudes and larger at high altitudes. Figure 5 is a plot of the ratio of measured to modeled [OH] versus altitude. As can be seen, at sea level the ratio is on average ~1.5, indicating that the model is underestimating [OH] compared to measurements. As altitude increases the average ratio drops to unity at ~0.8 km and then falls to a more or less constant value of ~0.8 at altitudes >2 km. It is this large number of measurements made above 2 km that is dominating the

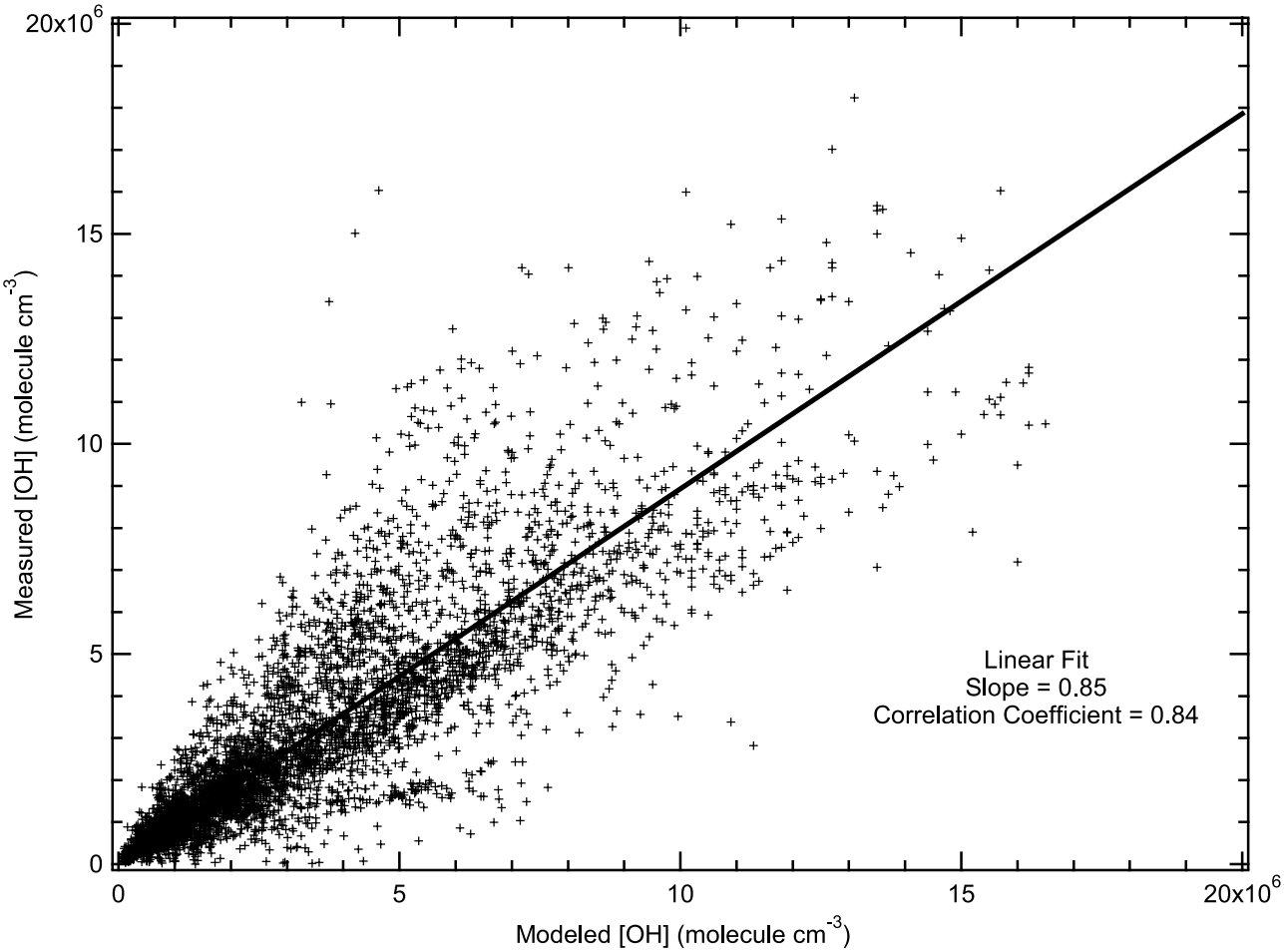

Figure 4. Comparison of measured OH values from the entire TRACE-P study together with those obtained from model simulations. A linear fit to this data yields a slope of 0.85 with a correlation coefficient of 0.84, indicating an overall tendency for the model to overestimate measurements.

fewer measurements below 2 km to give an overall agreement of 0.85–0.89, depending upon the regression used.

[17] Putting the present overall trend value of 0.85 (the slope from the same type of regression as used in these studies) into historical perspective, it compares well with the central pacific values of 0.86 and 0.80 obtained during the PEM-Tropics B study by *Tan et al.* [2001a] and *Mauldin et al.* [2001], respectively. This contrasts to the generally poor agreement with the continental values of 0.7, 0.5, and 0.38 obtained by *Carslaw et al.* [1999], *Carslaw et al.* [2001], and *Tan et al.* [2001b], respectively. When compared to the values obtained in the TOPSE study, the present value agrees with the value of 0.8 obtained at higher latitudes (>70°N) but does not agree very well with the value of 0.6, obtained at lower latitudes (<57°N) [*Mauldin et al.*, 2003]. The altitude trend of underestimating OH at low altitudes and overestimating OH at high altitudes in the model agreement has also been observed in previous studies [*Mauldin et al.*, 1999, 2001; *Tan et al.*, 2001a] and is also present in model simulations of OH data obtained aboard the DC-8 during TRACE-P [*Crawford et al.*, 2003]. An intercomparison of OH and other data obtained from both the P-3B and DC-8 aircraft during three close proximity flight legs can be found in the work of *Eisele et al.* [2003].

[18] As pointed out by *Mauldin et al.* [2003], *Tan et al.* [2001a, 2001b], and *Carslaw et al.* [2001, 1999, and references therein], the tendency for models to overestimate OH concentrations seems to be enhanced for measurements performed in continentally influenced air. One historically common explanation is the presence of one or more unaccounted for hydrocarbon compounds, perhaps oxygenated species, which act as OH sinks [*McKeen et al.*, 1997]. In continentally influenced regions, where biogenic carbon production is larger and transport of hydrocarbons and other compounds from local sources can increase the hydrocarbon loading, models begin to overestimate OH concentrations. What is interesting in this study is that while the measurements were performed over water, they were obtained in regions of continental outflow. One possibility for the better agreement in this region of continental influence, compared to other studies, is the addition of HO_2 and $HO_2 + RO_2$ measurements [*Cantrell et al.*, 2003] to the model. These two radicals are key species in the HO_x cycle, and the addition of their measurement is expected to improve OH simulations.

[19] One other possibility is that the lifetime(s) of this/these hypothesized unaccounted for hydrocarbon(s) is sufficiently short that they are substantially reduced or

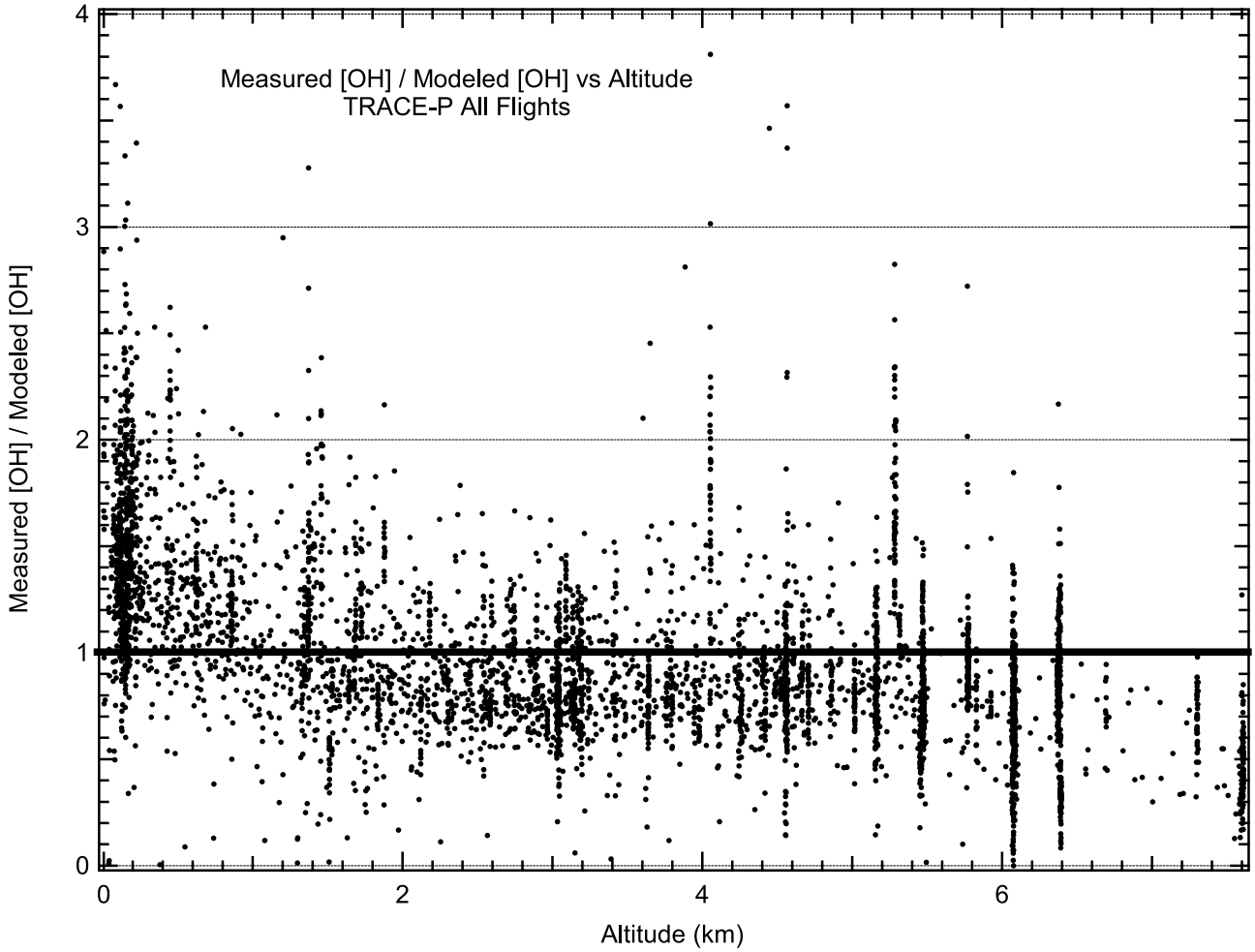

Figure 5. Plot of the ratio of measured to modeled OH versus altitude. As can be seen, the model tends to underpredict measured OH at altitudes <1.5 km. At altitudes >1.5 km the model tends to overestimate OH measurements. As the bulk of the measurements were made at altitudes >1.5 km, this overestimation dominates the overall model agreement seen in Figure 4.

removed during transport from the continent to out over the water. A quick test of the feasibility of this possibility can be performed by assuming pseudo-first-order conditions in which the [OH] remains constant and then estimating an equivalent rate coefficient for reaction with OH necessary to remove a hydrocarbon representative of the unaccounted for hydrocarbon specie(s) during transport. Here the lifetime of the representative hydrocarbon is the reciprocal of the apparent rate coefficient (the product of the [OH] and the second-order rate coefficient). A typically observed midday OH concentration of 3×10^6 molecule cm^{-3} equates to $\sim 1 \times 10^6$ molecule cm^{-3} when the diurnal cycle is averaged over 24 hours. If one assumes a transport time (hydrocarbon lifetime) from the continent to the measurement region of 0.5–1.5 days (reasonable for this study), second-order rate coefficients of 2.3×10^{-11}–7.7×10^{-12} cm^3 $molecule^{-1}$ s^{-1} are obtained for reaction with OH. These values fall in the range of rate coefficients for OH reacting with formaldehyde and OH reacting with propane, $\sim 1 \times 10^{-11}$ and $\sim 2.4 \times 10^{-13}$ cm^3 $molecule^{-1}$ s^{-1}, respectively. Thus it is possible that once the air mass has moved from the continental source regions, OH could have substantially reduced unmeasured hydrocarbon species during transport and thus their impact upon steady state OH concentrations in the measurement regions.

3.2. H_2SO_4 Measurements in Volcanic Plume

[20] The dynamic range of the instrument can be seen in the H_2SO_4 values from P-3B flight 17. Figure 6 (bottom) is a plot of the observed H_2SO_4 values from this flight together with SO_2, the primary source of H_2SO_4 in the troposphere. Also shown in Figure 6 (bottom) is a relative altitude profile for reference. This flight was flown to the southeast off the southern coast of Japan. During the flight a volcanic plume from Miyaka, Japan, was encountered in the boundary layer, characterized by large concentrations (>10 ppbv) of SO_2 and an absence of CO. As can be seen, the concentrations of H_2SO_4 during these periods are also extremely large with values greater than 10^8 molecule cm^{-3}. At these temperatures and humidities, these high concentrations of H_2SO_4 are usually accompanied by high concentrations of 3–4 and 3–8 nm particles indicating new particle formation [*Weber et al.*, 1995, 1999]. Shown in Figure 6 (top) is a plot of total (3 to ~200 nm) ultrafine condensation nuclei (UCN), 3–8 nm UCN, and 3–4 nm UCN. The total UCN values have been divided by 100 so

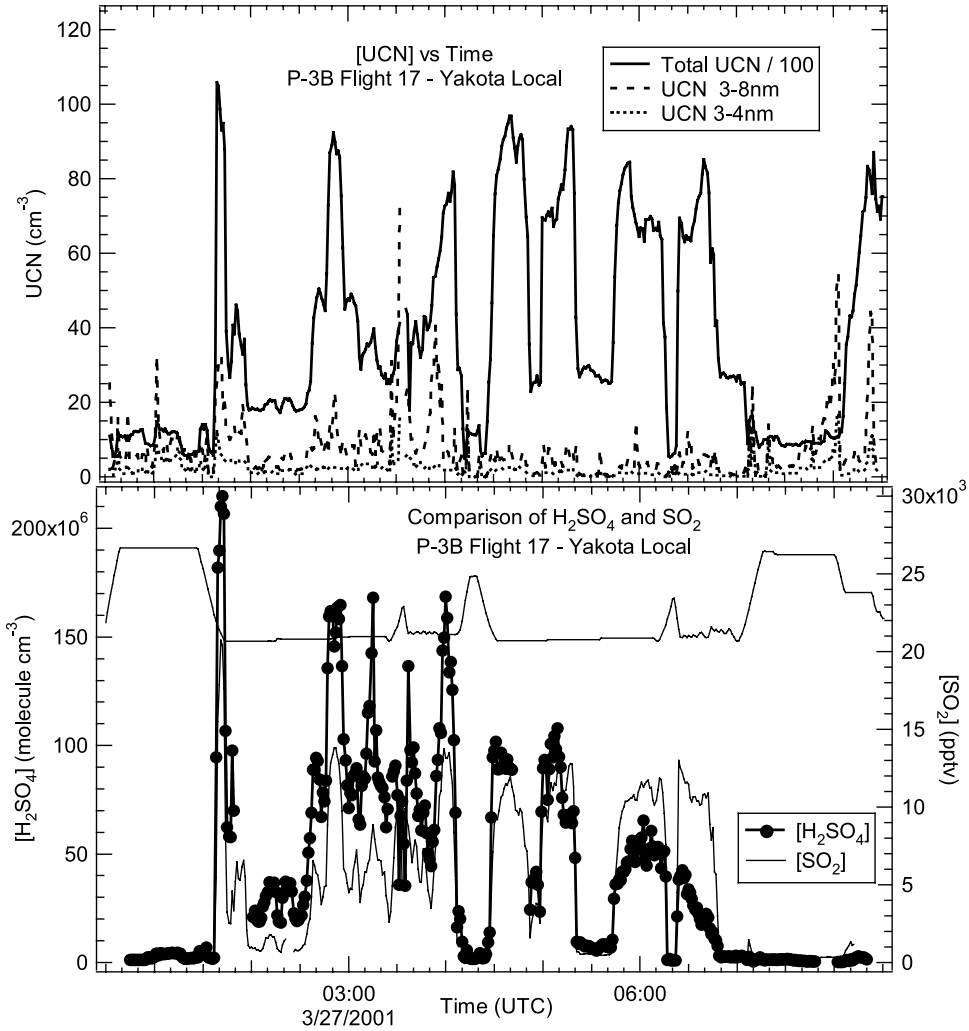

Figure 6. (bottom) Plot of $[H_2SO_4]$ and $[SO_2]$ for a flight in which a boundary layer volcanic plume from Miyaka, Japan, was encountered. A relative altitude profile (0.2–4.3 km) is provided for reference. As can be seen, both the $[SO_2]$ and $[H_2SO_4]$ are quite large during the encounters with the $[H_2SO_4]$ spiking to values greater than 10^8 molecule cm^{-3}. (top) Plot of total ultrafine condensation nuclei (UCN), 3–8 nm UCN, and 3–4 nm UCN for the same flight. The UCN values have been divided by 100 for scale purposes. The presence of the 3–4 nm and 3–8 nm spikes indicate the presence of newly formed particles.

that they would scale with the other UCN values. As can be seen, the total UCN is quite high with values greater than 8000 cm^{-3} during the plume encounters. During the extreme H_2SO_4 spikes the values of 3–4 nm and 3–8 nm UCN are also seen to rise, indicating the nucleation of new particles. The concentrations of 3–4 and 3–8 nm UCN are not as large as has been observed in cleaner environments [*Weber et al.*, 1995, 1999, 2003] because of the presence of a large number of preexisting particles. The presence of these particles increases the surface area to which the newly nucleated particles are exposed, enhancing the likelihood that the smaller particles will become incorporated into the larger ones, thus shortening the lifetime of the smaller, newly nucleated particles.

3.3. Nighttime Flight Off Midway Island

[21] An example of the precision the instrument is capable of when measuring low OH is P-3B flight 21, flown in the dark out of Midway Island. These types of flights are also good checks for possible interferences as OH concentrations are typically $<10^5$ molecule cm^{-3} during the night for remote environments. Figure 7a is a plot of the observed [OH] during this flight. Shown are the individual 30 s measurements and 5 min averages. Also shown is an altitude profile for reference. With the exception of some noisy excursions, it can be seen the 30 s values are $<2 \times 10^5$ molecule cm^{-3}, a typical limit of detection for a single measurement. Performing 5 min averages during these periods yield values $<5 \times 10^4$ molecule cm^{-3}.

[22] The noisy periods shown in Figure 7a are actually the indication of something quite unusual. The flight path was a straight line to the southwest, and a straight line return with boundary layer runs occurring at three fairly evenly spaced locations on the linear flight path. As can be seen from the altitude profile, the noisy periods occur during the portions of the flight flown in the boundary layer. Figure 7b

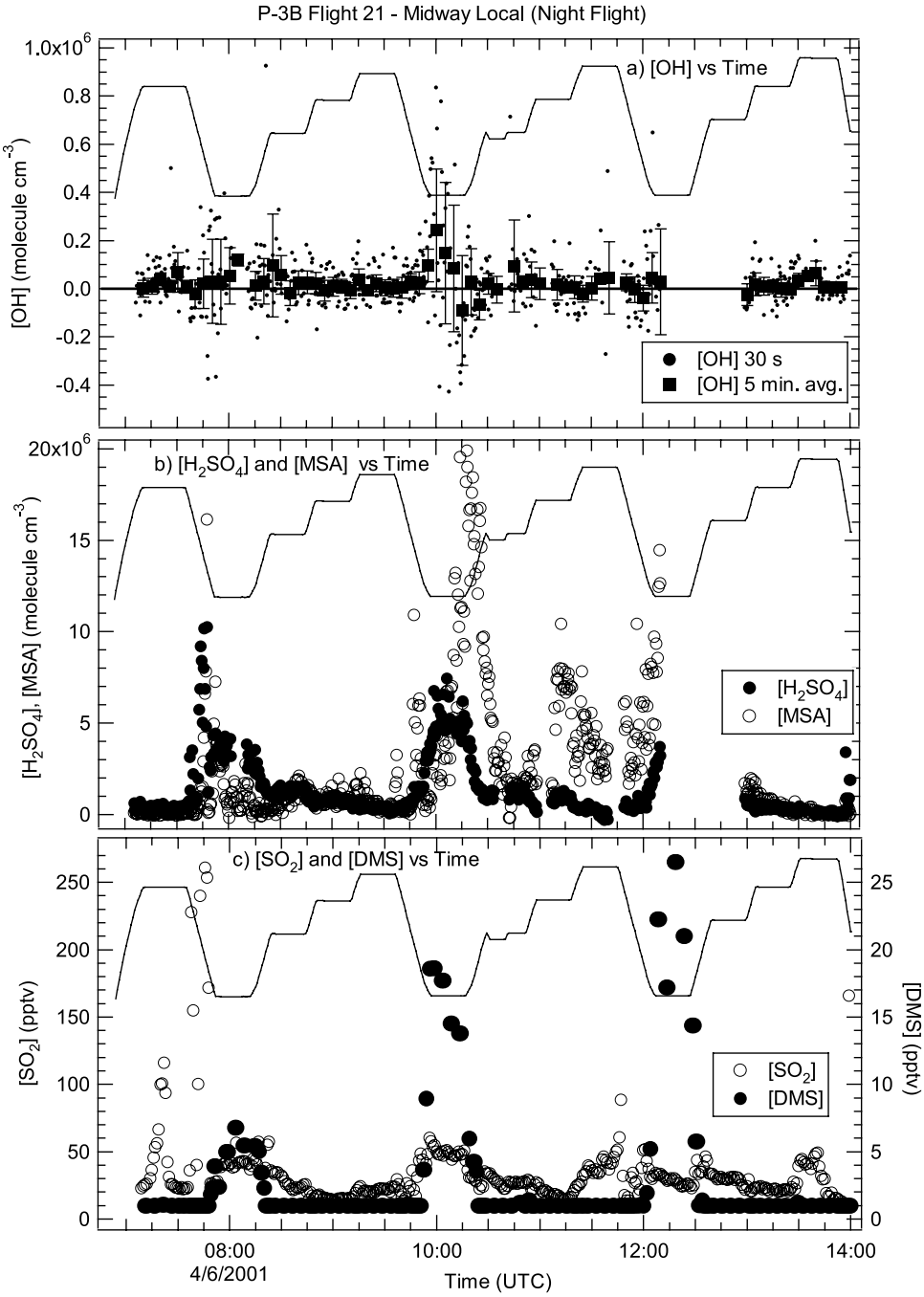

Figure 7. Measurements from a nighttime flight off Midway Island. Takeoff for this flight was ~1 hour after sunset. A relative altitude profile (0.5–6.7 km) is provided for reference. (a) Plot of observed [OH]. As can be seen, the values are quite small with typical 5 min averages $<2 \times 10^4$ molecule cm^{-3}. (b) Plot of observed $[H_2SO_4]$ and [MSA] for the same flight. The boundary layer concentration of these two short-lived, photochemically produced species is quite large for nighttime conditions. As the typical lifetimes of these compounds are short (<20 min), these concentration levels indicate production is occurring. (c) Plot of $[SO_2]$ and [DMS], two reactants known to produce H_2SO_4 and MSA. The SO_2 and H_2SO_4 measurements indicate that the oxidizing specie(s) is approximately as strong as OH (see text). Combining the very large boundary layer MSA concentrations with the rising concentrations, it is hard to explain that DMS is the primary reactant to form MSA.

is a plot of the H_2SO_4 and MSA concentrations from this same flight. As can be seen, both H_2SO_4 and MSA show a marked increase during these time periods, with H_2SO_4 reaching levels of $4–6 \times 10^6$ molecule cm^{-3} and MSA in excess of 10^7 molecule cm^{-3}. The fact that such large concentrations of these two relatively short-lived, photochemically produced species are observed during the night is quite remarkable. Takeoff for this flight was ~1 hour

after local sunset. Typical lifetimes for H_2SO_4 and MSA in a clean environment are ~20 min. The concentration levels of H_2SO_4 are on par with those seen during the day on the flights off Asia. Gas phase MSA concentrations such as these are typically only seen in much higher, dryer environments [*Mauldin et al.*, 1999].

[23] These observations raise the concern that the large values could be due to evaporation of H_2SO_4 and MSA from the inlet surfaces. Large increases in temperature or drops in relative humidity could cause an increase in the vapor pressure of H_2SO_4 or MSA absorbed on the surface of the 1.9 cm curved inlet. The effect of evaporation has been observed by our group only once before [*Mauldin et al.*, 1998], and then only at high altitude where the relative humidity fell below 5%. During the descents to these boundary layer runs, the temperature only changed by ~30°C going from approximately −10 to +20°C. The relative humidity during these boundary layer runs never fell below 80%. From the work of *Marti et al.* [1997], increasing the relative humidity from 5 to 80% decreases the vapor pressure of H_2SO_4 some 4 orders of magnitude. Field observations of MSA indicate that it has a similar but weaker response to relative humidity [*Mauldin et al.*, 1998]. Thus both previous flight experience with the inlet and laboratory measurements of H_2SO_4 vapor pressure would indicate that evaporation of H_2SO_4 and MSA is insignificant for the conditions of the boundary layer portions (or the rest) of this flight.

[24] Evidence of nighttime oxidation has been seen before [*Cantrell et al.*, 1997; *Hu and Steadman*, 1995; *Berresheim et al.*, 2002]. *Cantrell et al.* [1997] saw evidence of nighttime peroxy radical formation during the Mauna Loa Observatory Photochemistry Experiment (MLOPEX) 2c study. In that study the authors postulated NO_3 radical chemistry as a possible explanation for their results. As these measurements were performed in the remote marine boundary layer, NO_x/NO_y levels were low. Measurements aboard the P-3B revealed average values of 0, 5, and 200 pptv for NO, NO_2, and NO_y, respectively during the boundary layer segments, indicating little possibility for NO_3 formation. Additionally, rate coefficients show that NO_3 will not significantly react with SO_2 [*DeMore et al.*, 1997]. *Cantrell et al.* [1997] also suggested O_3 chemistry as another possible source of OH and ultimately peroxy radicals. This chemistry involves the reaction of O_3 with alkenes to forming a Criegee radical and ultimately OH. *Berresheim et al.* [2002] have observed the presence of H_2SO_4 and MSA at in the coastal marine boundary layer at Mace Head, Ireland. The authors reported average nighttime concentrations of H_2SO_4 of ~0.9×10^6 molecule cm^{-3} and performed experiments to show the presence of a specie(s) capable of oxidizing SO_2 into H_2SO_4. A mechanism involving either Criegee radicals or BrO, or both, was postulated. It is doubtful that the Criegee chemistry can explain the results of the present study. The OH measurements during the boundary layer portions are scattered about zero and never rise above 2.2×10^5 molecule cm^{-3}, a value far to low to maintain such high concentrations of H_2SO_4 and MSA. Additionally, as in the work of *Cantrell et al.* [1997], the measured concentrations of O_3 and alkenes during the boundary layer segments are too low to maintain the levels of H_2SO_4 and MSA observed. Data from the present study cannot confirm or rule out the possibility of oxidation involving halogen chemistry. The presence of MSA at night was explained by changes in mixing between the boundary layer and the mixed layer or free troposphere [*Berresheim et al.*, 2002]. Such mixing allows MSA produced from DMS at higher altitudes to be entrained within the marine boundary layer [*Davis et al.*, 1998; *Jefferson et al.*, 1998]. This mixing is usually accompanied by the passage of a weather front. Examination of the meteorology for the study region, revealed no frontal passage for at least 36 hours prior to the flight. This fact together with the relatively short lifetime of gas phase MSA would tend to indicate that mixing of this type could not contribute significantly to the observed MSA concentrations.

[25] In order to maintain these daytime like concentrations of these two relatively short-lived species, production of H_2SO_4 and MSA must be occurring. In the marine environment these two compounds are primarily produced via oxidation of reduced sulfur, emitted from the oceans primarily in the form of DMS [*Bates and Cline*, 1985; *Andreae et al.*, 1985]. Once in the atmosphere, DMS is oxidized by OH via a branched mechanism to produce either SO_2, much of which eventually forms H_2SO_4, or products which can lead to the formation of MSA, [*Ayers et al.*, 1991; *Yin et al.*, 1990; *Toon et al.*, 1987; *Hatakeyama et al.*, 1982]. Figure 7c is a plot of SO_2 and DMS concentrations also measured during this flight. As can be seen, both species exhibit concentration peaks during the boundary layer portions of the flight. The DMS concentrations are not large with boundary layer values increasing over time from ~5 to ~25 pptv. The SO_2 concentrations are also modest with values of ~50 pptv during all three boundary layer legs. The concentrations of both SO_2 and DMS, while small, do indicate the presence of two known reactants that, when oxidized via OH, produce H_2SO_4 and MSA, respectively. However, the key oxidizer, OH, is not present, and this oxidation is occurring at night.

[26] An interesting exercise is to perform a crude "equivalent OH" behavior calculation for this "mystery" nighttime oxidizer. If a daytime scenario is assumed with production of H_2SO_4 from SO_2 being in steady state equilibrium with its loss, an equivalent OH concentration can be obtained from the SO_2 and H_2SO_4 measurements, assuming H_2SO_4 is formed from OH + SO_2. Once formed, gas phase H_2SO_4 has an atmospheric lifetime on the order of an hour or less, being lost by condensation, rainout, or dry deposition. To properly calculate the H_2SO_4 lifetime, the particle surface area as a function of particle size needs to be known. Unfortunately, these values are not presently available, forcing the assumption of a H_2SO_4 lifetime. Here average respective SO_2 and H_2SO_4 concentrations of 1.23×10^9 (50 pptv) and 5×10^6 molecule cm^{-3} and a rate coefficient of 8.83×10^{-13} cm^2 $molecule^{-2}$ s^{-1} for OH + SO_2 + M → H_2SO_4 + M [*DeMore et al.*, 1997] were employed. H_2SO_4 lifetimes of <1 hour were assumed. Equivalent OH concentrations of $1.27–15.8 \times 10^6$ molecule cm^{-3} are obtained for H_2SO_4 lifetimes of 1 hour and 5 min, respectively, using this approach. While the equivalent OH value for a H_2SO_4 lifetime of 5 min (an extremely short lifetime) is large, lifetimes of 10 min to 1 hour yield values in the mid-10^6 molecule cm^{-3} range, on order with daytime measurements.

[27] Once formed in the gas phase, H_2SO_4 plays an important role in particle formation and growth. In areas

away from the Earth's surface, condensation of H_2SO_4 is thought to occur predominately on the surface of pre-existing aerosol particles [*Clarke et al.*, 1996; *Ayers et al.*, 1991]. However, gas phase H_2SO_4 is thought to initiate new particle formation, if the existing particle surface area is small [*Covert et al.*, 1992; *Hoppel et al.*, 1994]. As previously mentioned, UCN was also measured during this flight. An analysis of this data during the boundary layer runs not only reveals the presence of larger more aged UCN with diameters <200 nm but also the presence of 3–4 nm and 3–8 nm UCN, indicating recent particle nucleation at night.

[28] As stated above, the MSA concentrations observed during the boundary layer runs are more typical of higher, dryer environments. In the remote marine environment, gas phase MSA is thought to be produced from the oxidation of DMS via OH. This oxidation can proceed via abstraction or addition channels, both of which produce MSA [*Davis et al.*, 1998, 1999]. Other products include SO_2 (which ultimately forms H_2SO_4), dimethyl sulfoxide (DMSO), dimethyl sulfone ($DMSO_2$), and methane-sulfinic acid (MSIA). The overall temperature dependence of the reaction increases the final MSA/H_2SO_4 as the temperature decreases. Previous studies in areas with similar temperatures and much higher DMS production have yielded boundary layer daytime gas phase MSA concentrations on the order $<10^6$ molecule cm^{-3}, levels substantially lower than those observed here in the dark [*Mauldin et al.*, 1998, 1999, 2001]. Thus to maintain the concentration levels observed here, the production of gas phase MSA here at night must be greater than that from the OH + DMS reaction observed in those previous studies.

[29] Here two different possibilities can be considered: (1) the mechanism of DMS reacting with this nighttime oxidant is more efficient at producing MSA than the OH + DMS reaction, or (2) MSA is being produced via the oxidation of some other species. As the presence of this nighttime oxidant is only being inferred by the presence of short-lived oxidation products, any comment on a reaction mechanism with DMS would be speculation. However, there may be evidence that DMS is not the primary reactant. As can be seen from Figure 7c, the boundary layer concentration of DMS appears to be increasing over the evening, rising from 5 pptv on the first boundary layer leg, to 25 pptv on the last. The first and third legs were flown in the same area about 4 hours apart. This type of profile of DMS increasing over the evening has been observed before [*Davis et al.*, 1999; *Nowak et al.*, 2001], in an area with DMS production and little or no removal. Assuming DMS is the primary source of MSA, the rate of production (flux) DMS must be larger than the rate of removal by this nighttime oxidant for the same type of profile to be observed in the present study. This is a conclusion not out of the realm of possibility, however, it must be pointed out that it is a multistep reaction with OH that yields MSA from DMS, and presumably would be so with this nighttime oxidant.

[30] In the OH abstraction channel with DMS, MSA is produced via the formation of a CH_3S radical followed by reactions involving O_3, HO_2, or NO [*Davis et al.*, 1998]. The OH addition channel produces MSA via the formation of DMSO, followed by further reaction with OH. Comparing the rate coefficients for reaction with OH, one finds the DMSO rate coefficient is more than 100 times faster than that for DMS [*DeMore et al.*, 1997; *Hynes et al.*, 1986]. If the same holds factor holds true for the nighttime oxidant, it would take very little DMSO to produce the observed concentrations of MSA. The role of heterogeneous reactions could also be important in this oxidation. *Jefferson et al.* [1998] postulate that the large particulate concentrations of MSA observed during the ground-based Sulfur Chemistry in the Antarctic Troposphere Experiment (SCATE) study on the Palmer peninsula, Antarctica, were due to condensed phase oxidation of DMSO. The high solubility of DMSO and the low vapor pressure of MSA would tend to preclude these sorts of reactions as being strong gas phase sources of either compound.

[31] Recently, *Nowak et al.* [2001] have reported results from the GTE PEM-Tropics B study, indicating the possibility that DMSO may be produced at night. In that study the authors measured predawn boundary layer DMSO concentrations of 5–15 pptv. The DMSO concentration profiles were significantly out of phase with model predictions which assumed DMSO to be produced only from the OH initiated oxidation of DMS. In fact the measured diurnal DMSO profiles closely tracked the observed DMS profiles, increasing until the daylight hours and then decreasing. To reconcile differences between measurements and model predictions for the PEM-Tropics B study and to explain previous ground based DMSO observations, the authors point to an alternative DMSO source, possibly the ocean itself. The high solubility of DMSO in H_2O, makes it difficult to understand how the ocean can be a very large source of gas phase DMSO, except possibly during large sea spray events. In light of the present results, another possible explanation of the observations of *Nowak et al.* [2001] could be the formation of DMSO by the nighttime oxidation of DMS. There is some evidence of this possibility seen in the H_2SO_4 and MSA data obtained during the same PEM-Tropics B flight focused on by *Nowak et al.* [2001]. That flight was flown in the early morning such that the first boundary layer leg occurred around local sunrise. While not obtained in the dark, the H_2SO_4 and MSA concentrations were quite high for that time of day, with averages of $\sim 5 \times 10^6$ and $\sim 8 \times 10^6$ molecules cm^{-3}, respectively [*Mauldin et al.*, 2001]. Unfortunately, DMSO was not measured during the present study; thus its role in this nighttime oxidation chemistry remains speculative.

4. Summary and Conclusions

[32] Combined with other parameters measured aboard the P-3B, the OH data set presented here allows an extensive comparison with model simulations over a broad range of ambient conditions. The overall average model agreement value of 0.85 is very similar to the values of 0.80 and 0.86 observed during the PEM-Tropics B study [*Tan et al.*, 2001a; *Mauldin et al.*, 2001]. As the bulk of the measurements were performed in areas of Asian outflow, it is surprising that the agreement is quite better than the continental values of 0.7, 0.5, and 0.38 obtained by *Carslaw et al.* [1999], *Carslaw et al.* [2001], and *Tan et al.* [2001b], respectively.

[33] Similarly, the H_2SO_4 values provided allow a somewhat complete analysis of sulfur oxidation chemistry going from the initial reactant of SO_2 to the final product of UCN particles. The levels of H_2SO_4 encountered in the boundary layer during the volcanic plume represent some of the largest values observed in the marine boundary layer.

[34] The observation of high levels of H_2SO_4 and MSA during the night is quite interesting. As these are two short-lived species, the concentrations observed indicate that significant production of these species is occurring. Measurable quantities of SO_2 and DMS, two compounds which when oxidized produce H_2SO_4 and MSA, were observed; however, OH concentrations during these periods were essentially zero. While evidence of nighttime oxidation has been observed before in the coastal marine boundary layer [*Berresheim et al.*, 2002], the finding of evidence in the remote marine boundary layer is unique. From the results presented it would appear that this yet to be determined oxidant has a reactivity on the order of that of OH. The large concentrations of MSA observed in themselves present a question regarding a possible mechanism. Known DMS oxidation chemistry involving OH cannot account for the MSA to H_2SO_4 ratios observed. While not measured, the high reactivity, and easier avenue to MSA, makes DMSO a more likely candidate as the direct source. Recent work by *Nowak et al.* [2001] has demonstrated the likelihood that DMSO is produced at night, possibly by the ocean itself. As pointed out by these authors, the high solubility of DMSO makes it difficult to see how that mechanism could explain the observed gas phase DMSO values. A possible mechanism which could explain the results of *Nowak et al.* [2001] and those of the present study would be the formation of DMSO from the nighttime oxidation of DMS. This DMSO could be further oxidized to form MSA. To explain the observed boundary layer MSA/H_2SO_4 ratios, this oxidant must be more efficient at producing DMSO (and ultimately MSA) from DMS than is OH. These observations only add to the already complicated puzzle of marine boundary layer chemistry.

[35] **Acknowledgments.** The authors would like to express their thanks to the NASA Wallops Flight Facility for their help and logistical support. We would also like to thank Bruce Henry of NCAR/ACD for his help with the data analysis. NCAR is supported by the NSF.

References

Andreae, M. O., R. J. Ferek, F. Bermond, K. P. Byrd, R. T. Engstrom, S. Hardin, P. D. Houmere, F. LeMarrec, and H. Raemdonck, Dimethyl sulfide in the marine atmosphere, *J. Geophys. Res.*, *90*, 12,891–12,900, 1985.

Ayers, G. P., J. P. Ivey, and R. W. Gillett, Coherence between seasonal cycles of dimethyl sulfide, methane sulfonate, and sulfate in marine air, *Nature*, *349*, 404–406, 1991.

Bates, T. S., and J. D. Cline, The role of the ocean in a regional sulfur cycle, *J. Geophys. Res.*, *90*, 9168–9172, 1985.

Berresheim, H., T. Elste, H. G. Tremmel, A. G. Allen, H.-C. Hansson, K. Rosman, M. Dal Maso, J. M. Mäkelä, M. Kulmala, and C. D. O'Dowd, Gas-aerosol relationships of H_2SO_4, MSA, and OH: Observations in the coastal marine boundary layer at Mace Head, Ireland, *J. Geophys. Res.*, *107*(D19), 8100, doi:10.1029/2000JD000229, 2002.

Cantrell, C. A., G. Tyndall, and A. Zimmer, Absorption cross-section for water vapor from 183 to 193 nm, *J. Geophys. Res.*, *24*, 2195–2198, 1997.

Cantrell, C. A., et al., Peroxy radical behavior during Transport and Chemical Evolution over the Pacific as measured aboard the NASA P-3B aircraft, *J. Geophys. Res.*, *108*(D2), 8797, doi:10.1029/2003JD003674, in press, 2003.

Carslaw, N., D. J. Creasey, D. E. Heard, A. C. Lewis, J. B. McQuaid, M. J. Pilling, P. S. Monks, B. J. Bandy, and S. A. Penkett, Modeling OH, HO_2, and RO_2 radicals in the marine boundary layer: 1. Model construction and comparison with field measurements, *J. Geophys. Res.*, *104*, 30,241–30,255, 1999.

Carslaw, N., et al., OH and HO_2 radical chemistry in a forested region of north-western Greece, *Atmos. Environ.*, *35*, 4725–4737, 2001.

Charlson, R. J., J. E. Lovelock, M. O. Andreae, and S. G. Warren, Ocean phytoplankton, atmospheric sulfur, cloud albedo and climate, *Nature*, *326*, 655–661, 1987.

Clarke, A. D., Z. Li, and M. Litchy, Aerosol dynamics in the equatorial Pacific marine boundary layer: Microphysics, diurnal cycles, and entrainment, *Geophys Res. Lett.*, *23*, 733–736, 1996.

Covert, D. S., V. N. Kapustin, P. K. Quinn, and T. S. Bates, New particle formation in the marine boundary layer, *J. Geophys. Res.*, *97*, 20,581–20,589, 1992.

Crawford, J., et al., Clouds and trace gas distributions during Transport and Chemical Evolution over the Pacific, *J. Geophys. Res.*, *108*(D21), 8818, doi:10.1029/2002JD003177, in press, 2003.

Creasey, D. J., D. E. Heard, and J. D. Lee, Absorption cross-section measurements of water vapor and oxygen at 185 nm: Implications for the calibration of field instruments to measure OH, HO_2, and RO_2 radicals, *Geophys. Res. Lett.*, *27*, 1651–1654, 2000.

Davis, D., G. Chen, P. Kasibhatla, A. Jefferson, D. Tanner, F. Eisele, D. Lenschow, W. Neff, and H. Berresheim, DMS oxidation in the Antarctic marine boundary layer: Comparison of model simulations and field observations of DMS, DMSO, $DMSO_2$, H_2SO_4(g), MSA(g), and MSA(p), *J. Geophys. Res.*, *103*, 1657–1678, 1998.

Davis, D., et al., Dimethyl sulfide oxidation in the equatorial Pacific: Comparison of model simulations with field observations for DMS, SO_2, H_2SO_4(g), MSA(g), MS, and NSS, *J. Geophys. Res.*, *104*, 5765–5784, 1999.

DeMore, W. B., S. P. Sander, D. M. Golden, R. F. Hampson, M. J. Kurylo, C. J. Howard, A. R. Ravishankara, C. E. Kolb, and M. J. Molina, Chemical kinetics and photochemical data for use in stratospheric modeling, *JPL Publ.*, *97-4*, 13–126, 1997.

Eisele, F. L., and D. J. Tanner, Ion-assisted tropospheric OH measurements, *J. Geophys. Res.*, *96*, 9295–9308, 1991.

Eisele, F. L., and D. J. Tanner, Measurement of the gas phase concentration of H_2SO_4 and methane sulfonic acid and estimates of H_2SO_4 production and loss in the atmosphere, *J. Geophys. Res.*, *98*, 9001–9010, 1993.

Eisele, F., et al., Summary of measurement intercomparisons during Transport and Chemical Evolution over the Pacific, *J. Geophys. Res.*, *108*(D20), 8791, doi:10.1029/2002JD003167, 2003.

Hatakeyama, S., M. Okuda, and H. Akimoto, Formation of sulfur dioxide and methane sulfonic acid in the photooxidation of dimethyl sulfide in the air, *Geophys. Res. Lett.*, *9*, 583–586, 1982.

Hofzumahaus, A., et al., Reply to Comment by E. J. Lanzendorf et al. on "The measurements of tropospheric OH radicals by laser-induced fluorescence spectroscopy during the POPCORN field campaign" by Hofzumahaus et al. and "Intercomparison of tropospheric OH radical measurements by multiple folded long-path laser absorption and laser-induced fluorescence" by Brauers et al., *Geophys. Res. Lett.*, *24*, 3039–3040, 1997.

Hoppel, W. A., G. M. Frick, J. W. Fitzgerald, and R. E. Larson, Marine boundary layer measurements of new particle formation and the effects nonprecipitating clouds have on aerosol size distributions, *J. Geophys. Res.*, *99*, 14,443–14,459, 1994.

Hu, J., and D. H. Steadman, Atmospheric RO_x radicals at an urban site: Comparison to a simple theoretical model, *Environ. Sci. Technol.*, *29*, 1655–1659, 1995.

Hynes, A. J., P. H. Wine, and D. H. Semmes, Kinetics and mechanism of OH reactions with organic sulfides, *J. Phys. Chem.*, *90*, 4148–4156, 1986.

Jacob, D. J., J. Crawford, M. M. Kleb, V. S. Connors, R. J. Bendura, J. L. Raper, G. W. Sachse, J. Gille, L. Emmons, and J. C. Heald, Transport and Chemical Evolution over the Pacific mission: Design, execution, and first results, *J. Geophys. Res.*, *108*(D20), 8781, doi:10.1029/2002JD003276, 2003.

Jefferson, A., D. J. Tanner, F. L. Eisele, D. D. Davis, G. Chen, J. Crawford, J. W. Huey, A. L. Torres, and H. Berresheim, OH photochemistry and methane sulfonic acid formation in the coastal Antarctic boundary layer, *J. Geophys. Res.*, *103*, 1647–1656, 1998.

Lanzendorf, E. J., T. F. Hanisco, N. M. Donohue, and P. O. Wennberg, Comment on "The measurement of tropospheric OH radicals by laser-induced fluorescence spectroscopy during the POPCORN field campaign" by Hofzumahaus et al. and "Intercomparison of tropospheric OH radical measurements by multiple folded long-path laser absorption and laser-induced fluorescence" by Brauers et al., *Geophys. Res. Lett.*, *24*, 3037–3038, 1997.

Marti, J. J., A. Jefferson, X. P. Cai, C. Richert, P. H. McMurry, and F. Eisele, H_2SO_4 vapor pressure of sulfuric acid and ammonium sulfate solutions, *J. Geophys. Res.*, *102*, 3725–3735, 1997.

Mauldin, R. L., III, D. J. Tanner, G. J. Frost, G. Chen, A. S. H. Prevot, D. D. Davis, and F. L. Eisele, OH measurements during First Aerosol Characterization Experiment (ACE-1): Observations and model comparisons, *J. Geophys. Res.*, *103*, 16,713–16,729, 1998.

Mauldin, R. L., III, D. J. Tanner, and F. L. Eisele, Measurements of OH during PEM-Tropics A, *J. Geophys. Res.*, *104*, 5817–5827, 1999.

Mauldin, R. L., III, et al., Measurements of OH aboard the NASA P-3 during PEM-Tropics B, *J. Geophys. Res.*, *106*, 32,657–32,666, 2001.

Mauldin, R. L., III, C. A. Cantrell, M. A. Zondlo, E. Kosciuch, B. A. Ridley, R. Weber, and F. E. Eisele, Measurements of OH, H_2SO_4, and MSA during Tropospheric Ozone Production About the Spring Equinox (TOPSE), *J. Geophys. Res.*, *108*(D4), 8366, doi:10.1029/2002JD002295, 2003.

McKeen, S. A., et al., Photochemical modeling of hydroxyl and its relationship to other species during the tropospheric OH photochemistry experiment, *J. Geophys. Res.*, *102*, 6467–6493, 1997.

Nowak, J. B., et al., Airborne observations of DMSO, DMS, and OH at marine tropical latitudes, *Geophys. Res. Lett.*, *28*, 2201–2204, 2001.

Tan, D., et al., OH and HO_2 in the tropical Pacific: Results from PEM-Tropics B, *J. Geophys. Res.*, *106*, 32,667–32,681, 2001a.

Tan, D., et al., HO_x budgets in a deciduous forest: Results from the PROPHET summer 1998 campaign, *J. Geophys. Res.*, *106*, 24,407–24,427, 2001b.

Tanner, D. J., A. Jefferson, and F. L. Eisele, Selected ion chemical ionization mass spectrometric measurement of OH, *J. Geophys. Res.*, *102*, 6415–6425, 1997.

Toon, O. B., J. F. Kasting, R. P. Turco, and M. S. Liu, The sulfur cycle in the marine atmosphere, *J. Geophys. Res.*, *92*, 943–963, 1987.

Twomey, S. A., M. Piepgrass, and L. T. Wolfe, An assessment of the impact of pollution on global cloud albedo, *Tellus, Ser. B*, *36*, 356–366, 1984.

Weber, R. J., J. J. Marti, P. H. McMurry, F. L. Eisele, D. J. Tanner, and A. Jefferson, Measurements of expected nucleation precursor species and 3 to 500 nm diameter particles at Mauna Loa Observatory, Hawaii, *J. Geophys. Res.*, *101*, 14,767–14,775, 1995.

Weber, R. J., P. H. McMurry, R. L. Mauldin III, D. J. Tanner, F. L. Eisele, A. D. Clarke, and V. N. Kapustin, New particle formation in the remote troposphere: A comparison of observations at various sites, *Geophys. Res. Lett.*, *26*, 307–310, 1999.

Weber, R. J., et al., New particle formation in anthropogenic plumes advecting from Asia observed during Transport and Chemical Evolution over the Pacific, *J. Geophys. Res.*, *108*(D21), 8814, doi:10.1029/2002JD003112, in press, 2003.

Yin, F., D. Grosjean, R. C. Flagan, and J. H. Seinfeld, Photooxidiation of DMS and DMDS, II, mechanism evaluation, *J. Atmos. Chem.*, *11*, 365–399, 1990.

A. Bandy and D. Thornton, Department of Chemistry, Drexel University, Philadelphia, PA 19104, USA. (bandyar@drexel.edu; thorntdc@drexel.edu)

D. Blake, Department of Chemistry, University of California, Irvine, Irvine, CA 92697-2025, USA. (drblake@uci.edu)

C. A. Cantrell, F. L. Eisele, E. Kosciuch, and R. L. Mauldin III, Atmospheric Chemistry Division, National Center for Atmospheric Research, Boulder, CO 80303, USA. (cantrell@ncar.ucar.edu; eisele@ucar.edu; mauldin@acd.ucar.edu)

G. Chen and J. Crawford, NASA Langley Research Center, Hampton, VA, USA.

D. Davis and R. Weber, School of Earth and Atmospheric Sciences, Georgia Institute of Technology, Atlanta, GA 30332, USA. (rweber@eas.gatech.edu)

M. Zondlo, Southwest Sciences, Inc., 1570 Pacheco Street, Suite E-11, Santa Fe, NM 87505, USA. (mzondlo@swsciences.com)